Journal of Solid State Chemistry 225 (2015) 193–201

Contents lists available at ScienceDirect

Journal of Solid State Chemistry

journal homepage: www.elsevier.com/locate/jssc

The Ho–Ni–Ge system: Isothermal section and new rare-earth nickel germanides

A.V. Morozkin [a,*], A.V. Knotko [a], V.O. Yapaskurt [b], Fang Yuan [c], Y. Mozharivskyj [c], M. Pani [d], A. Provino [d], P. Manfrinetti [d]

[a] Department of Chemistry, Moscow State University, Leninskie Gory, House 1, Building 3, GSP-2, Moscow 119992, Russia
[b] Department of Petrology, Faculty of Geology, Moscow State University, Leninskie Gory, Moscow 119992, Russia
[c] Department of Chemistry and Chemical Biology, McMaster University, 1280 Main Street West, Hamilton, Ontario L8S 4M1, Canada
[d] Institute SPIN-CNR and Dipartimento di Chimica e Chimica Industriale, Università di Genova, Via Dodecaneso 31, 16146 Genova, Italy

ARTICLE INFO

Article history:
Received 3 November 2014
Received in revised form
17 December 2014
Accepted 21 December 2014
Available online 5 January 2015

Keywords:
Ho–Ni–Ge Phase diagram
Rare-earth compounds
Crystal structure
Magnetic properties

ABSTRACT

The Ho–Ni–Ge system has been investigated at 1070 K and up to ~60 at% Ho by X-ray diffraction and microprobe analyses. Besides the eight known compounds, $HoNi_5Ge_3$ (YNi_5Si_3-type), $HoNi_2Ge_2$ ($CeAl_2Ga_2$-type), Ho_2NiGe_6 (Ce_2CuGe_6-type), $HoNiGe_3$ ($SmNiGe_3$-type), $HoNi_{0.2\div0.6}Ge_2$ ($CeNiSi_2$-type), $Ho_{37\div34}Ni_{6\div24}Ge_{57\div42}$ (AlB_2-type), HoNiGe (TiNiSi-type), Ho_3NiGe_2 (La_3NiGe_2-type), the ternary system contains four new compounds: $Ho_3Ni_{11}Ge_4$ ($Sc_3Ni_{11}Ge_4$-type), $HoNi_3Ge_2$ ($ErNi_3Ge_2$-type), $Ho_3Ni_2Ge_3$ ($Hf_3Ni_2Si_3$-type) and ~$Ho_5Ni_2Ge_3$ (unknown structure). Quasi-binary solid solutions were observed at 1070 K for Ho_2Ni_{17}, $HoNi_5$, $HoNi_7$, $HoNi_3$, $HoNi_2$, HoNi and Ho_2Ge_3, but no detectable solubility was found for the other binary compounds in the Ho–Ni–Ge system. Based on the magnetization measurements, the $HoNi_5Ge_3$, $HoNi_3Ge_2$ and $Ho_3Ni_{11}Ge_4$ (and isostructural $\{Tb, Dy\}_3Ni_{11}Ge_4$) compounds have been found to show paramagnetic behavior down to 5 K, whereas $Ho_3Ni_2Ge_3$ exhibits an antiferromagnetic transition at ~7 K. Additionally, the crystal structure of the new isostructural phases $\{Y, Yb\}Ni_3Ge_2$ ($ErNi_3Ge_2$-type), $Er_3Ni_{11}Ge_4$ ($Sc_3Ni_{11}Ge_4$-type) and $\{Y, Tb, Dy, Er, Tm\}_3Ni_2Ge_3$ ($Hf_3Ni_2Si_3$-type) has been also investigated.

1. Introduction

An important step in addressing both fundamental and practical goals in the materials science, solid state chemistry and physics is the study of phase diagrams or isothermal cross-sections and determination of crystal structures of compounds formed in these systems. The knowledge of the phase equilibria allows to prepare samples with minimal or no impurities and to grow crystals by flux methods. Additionally, such knowledge can be used to predict phase equilibria and isostructural phases in analogous systems. The rare earth–Ni–Ge systems have already been extensively investigated, in terms of the isothermal sections and crystal structures of the ternary phases, for rare earth = Sc, Y, La–Nd, Tb, Dy, Tm, Lu, Yb [1–22]. One of the missing members of this family is the Ho–Ni–Ge system, which is the subject of the current work.

The constituent Ho–Ni, Ho–Ge and Ni–Ge binary systems have been studied in Ref. [9–12,23–26]; the crystal structure of the ternary compounds $HoNi_5Ge_3$ [13], $HoNi_2Ge_2$ [14], $HoNiGe_3$ [15], $HoNi_{0.6}Ge_2$ [16], Ho_2NiGe_6 [17], HoNiGe [18], $HoNi_{0.5}Ge_{1.5}$ [19] and Ho_3NiGe_2 [20] has been also established. Except for the $HoNi_5Ge_3$ phase, the magnetic properties of all the ternary phases $HoNi_2Ge_2$ [28], Ho_2NiGe_6 [29], HoNiGe [30], $HoNi_{0.6}Ge_2$ [39], $HoNi_{0.5}Ge_{1.5}$ [19], Ho_3NiGe_2 [31] and $HoNiGe_3$ [38] have been investigated as well. Furthermore, the following compounds $\{Er, Tm\}Ni_3Ge_2$ [5,21], $\{Sc, Y, Tb, Dy, Tm–Lu\}_3Ni_{11}Ge_4$ [4–8] and $Lu_3Ni_2Ge_3$ [22] were already found to form in the rare earth–Ni–Ge systems.

In this work, we present the isothermal section of the Ho–Ni–Ge system, along with crystal structure and magnetic properties of the new ternary phases $HoNi_3Ge_2$, $Ho_3Ni_{11}Ge_4$ and $Ho_3Ni_2Ge_3$. New isotypic rare earth–nickel–germanide phases formed with other heavy rare earths and magnetic properties of known $Sc_3Ni_{11}Ge_4$-type $\{Tb, Dy\}_3Ni_{11}Ge_4$ are also reported.

2. Experimental details

The samples with a total mass of 2–3 g were prepared by arc-melting on a water-cooled copper hearth (90 V, 150 A) under pure argon (99.992 vol%) and using a non-consumable tungsten electrode.

* Corresponding author.
E-mail address: morozkin@tech.chem.msu.ru (A.V. Morozkin).

http://dx.doi.org/10.1016/j.jssc.2014.12.025
0022-4596/

Pieces of germanium (purity 99.99 wt%), nickel (99.95 wt%) and rare earths (99.9 wt%) were used as starting materials. Titanium was used as a getter during arc-melting. The arc-melted samples were annealed at 1070 K (± 5 K) for 8–10 days in sealed quartz ampoules under low pressure of argon and then quenched in ice-cold water.

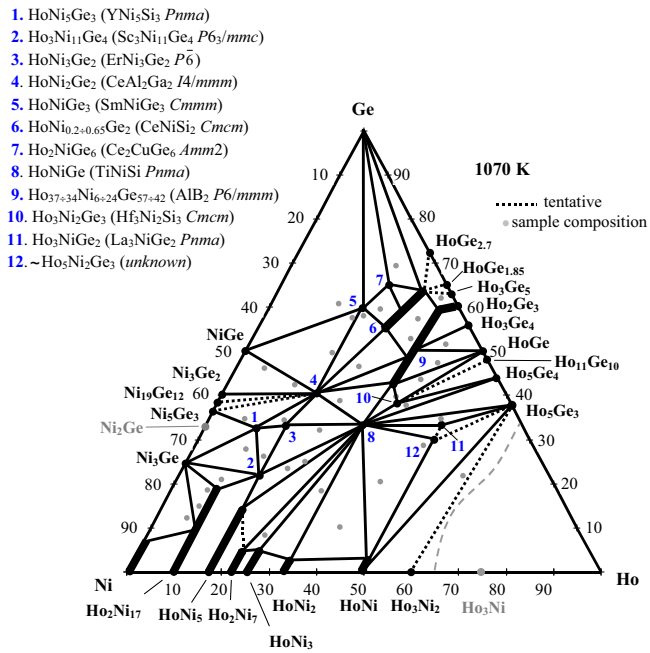

Fig. 1. Isothermal section of the Ho–Ni–Ge system at 1070 K.

Purity of the alloys and composition of the phases were evaluated using X-ray diffraction and electron microprobe analysis. The X-ray powder data were collected on a Rigaku d/max-2500 diffractometer (Cu*K*α radiation, 2θ range of 5–120 and 10–80°, step 0.02°, and 4–6 s/step). The unit cell parameters were derived from the Rietveld analysis [32] using the Rietan program in the isotropic approximation; the symmetry analysis was performed with the aid of the Bilbao Crystallographic Server [33].

An INCA-Energy-350 X-ray EDS spectrometer (Oxford Instruments) on the Jeol JSM-6480LV scanning electron microscope (20 kV accelerating voltage, 0.7 nA beam current and 50 μm beam diameter) was employed for the quantitative microprobe analyses. From signals averaged over three points we obtained the estimated standard deviations of 1 at% for all the three elements (rare earths measured by L-series lines; Ni and Ge measured by K-series lines) in all the phases.

The DC magnetization of polycrystalline samples was measured on a commercial SQUID magnetometer (Quantum Design) in the temperatures range of 5–300 K and applied field of 100 Oe. The effective magnetic moments and paramagnetic temperature were obtained by fitting the data to the Curie–Weiss law in the paramagnetic region [34].

3. Results

3.1. Ho–Ni–Ge system at 1070 K

Based on the X-ray and microprobe results, the isothermal section of the Ho–Ni–Ge system at 1070 K (up to ~60 at% Ho) has been determined (Fig. 1). Compositions of the samples prepared are shown as dots in Fig. 1. The solid lines were constructed by

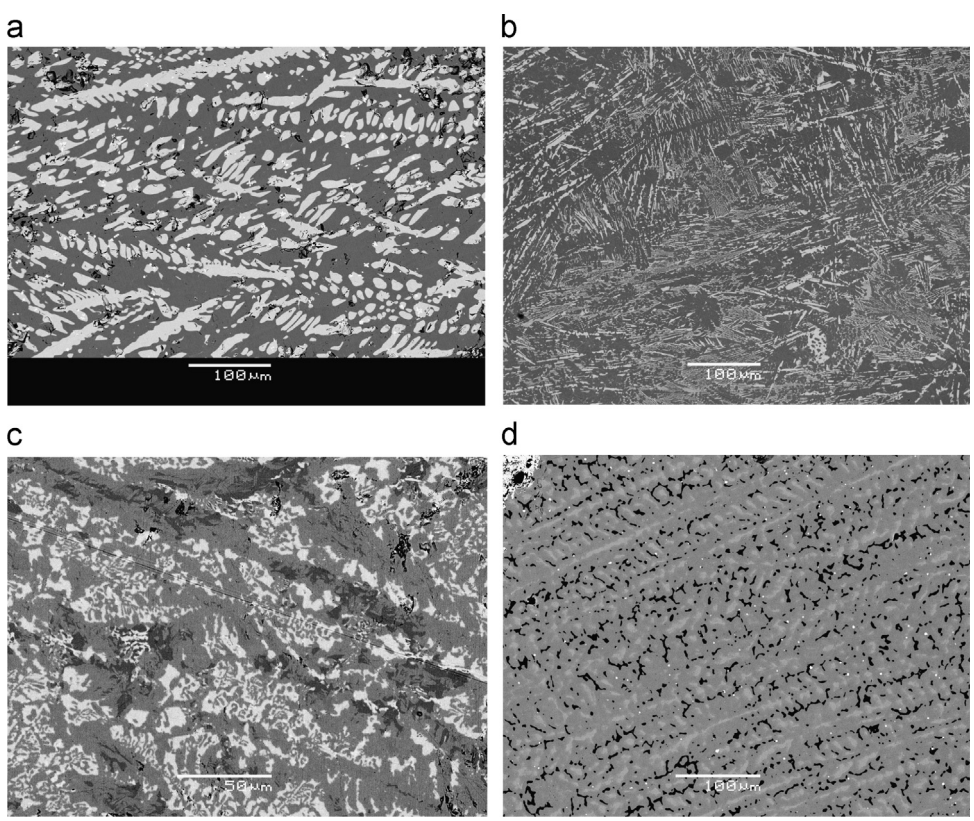

Fig. 2. Microstructure of some Ho–Ni–Ge samples after annealing at 1070 K for a 200 h: (a) '$Ho_{25}Ni_{40}Ge_{35}$': $Ho_{34}Ni_{33}Ge_{33}$ (TiNiSi-type) (white) and '$Ho_{21}Ni_{44}Ge_{35}$' (mixture of $CeAl_2Ga_2$-type $HoNi_2Ge_2$ and TiNiSi-type HoNiGe) (gray), (b) '$Ho_{40}Ni_{10}Ge_{50}$': $Ho_{50}Ge_{50}$ (CrB-type) (white needlese), $Ho_{44}Ge_{56}$ (Gd_3Ge_4-type) (white plates) and $Ho_{38}Ni_{12}Ge_{50}$ (AlB_2-type) (gray); (c) '$Ho_{40}Ni_{20}Ge_{40}$': $Ho_{51}Ge_{49}$ (CrB-type) (white), $Ho_{38}Ni_{25}Ge_{37}$ ($Hf_3Ni_2Si_3$-type) (gray) and $Ho_{34}Ni_{24}Ge_{42}$ (AlB_2-type) (black) and (d) '$Ho_8Ni_{80}Ge_{12}$': $Ho_{11}Ni_{78}Ge_{11}$ (Th_2Ni_{17}-type) (white gray), $Ni_{76}Ge_{34}$ ($AuCu_3$-type) (black gray) and $Ni_{91}Ge_9$ (Cu-type) (black).

combining the experimental microprobe EDX data with X-ray powder diffraction results. In few cases only, the tie lines and triangles were estimated and tentatively assigned. Fig. 2.

The known binary compounds and new pseudo-binary solid solutions belonging to the isothermal section at 1070 K are summarized in Table 1. Extended solid solutions were detected for the Ho_2Ni_{17}, $HoNi_5$, Ho_2Ni_7, $HoNi_3$, $HoNi_2$, HoNi and Ho_2Ge_3 binaries; no detectable solid solutions could be observed for the other binary compounds in the Ho–Ni–Ge system.

The known $HoNi_5Ge_3$, $HoNi_2Ge_2$, $HoNiGe_3$, $HoNi_{0.6}Ge_2$, Ho_2NiGe_6, HoNiGe, $HoNi_{0.5}Ge_{1.5}$ and Ho_3NiGe_2 ternary compounds were confirmed in the isothermal section at 1070 K. Furthermore, according to the microprobe analysis, the four new ternary phases with compositions $Ho_3Ni_{11}Ge_4$, $HoNi_3Ge_2$, $Ho_3Ni_2Ge_3$ and $\sim Ho_5Ni_2Ge_3$

Table 1
Lattice parameters of the binary compounds and their solid solutions in the Ho–Ni–Ge system (the phases belonging to the isothermal section at 1070 K are shaded, HT and LT are the high-temperature and low-temperature phase, respectively).

N	Compound	Space group	Type structure	*a* (nm)	*b* (nm)	*c* (nm)	R_F (%)	Refs.
1	Ho_{LT}	$P6_3/mmc$	Mg	0.35773		0.56158		[9,12,27]
	Ho_{HT}	$Im\bar{3}m$	W	0.39600				[9,12,27]
2	Ni	$Fm\bar{3}m$	Cu	0.35238				[9,12,27]
	$Ni_{92}Ge_8$	$Fm\bar{3}m$	Cu	0.3540				[12,23,24]
	$Ni_{91}Ge_9$	$Fm\bar{3}m$	Cu	0.3745(1)			2.8	[a]
3	Ge	$Fd\bar{3}m$	C	0.565754				[9,12,27]
	Ge	$Fd\bar{3}m$	C	0.56570(9)			8.2	[a]
4	Ni_3Ge	$Pm\bar{3}m$	$AuCu_3$	0.3566				[9–12,23,24]
	Ni_3Ge	$Pm\bar{3}m$	$AuCu_3$	0.35718(3)			4.0	[a]
	Ni_3Ge_{HT}	$Fd\bar{3}m$	NaTl	0.57436				[9–12,23,24]
5	Ni_5Ge_2	$P6_3/mmc$	Pd_5Sb_2	0.6827		1.2395		[9–12,23,24]
6	Ni_2Ge	$Pnma$	Co_2Si	0.5113	0.3830	0.7264		[9–12,23,24]
	Ni_2Ge	$C2/m$	x	1.0130	0.7800 $\beta = 90.4°$	0.6830		[9–12,23,24]
7	Ni_5Ge_3	$P6_3/mmc$	NiAs	0.3955		0.5046		[9–12,23,24]
	Ni_5Ge_3	$C2$	Ni_5Ge_3	1.1682	0.6737 $\beta = 52.11°$	0.6264		[9–12,23,24]
8	$Ni_{19}Ge_{12\ HT}$	$C2$	$Ni_{19}Ge_{12}$	1.1631	0.6715 $\beta = 90°$	1.0048		[9–12,23,24]
9	Ni_3Ge_2	$P6_3/mmc$	NiAs	0.3860		0.5000		[9–12,23,24]
	$Ni_{57}Ge_{43}$	$P6_3/mmc$	NiAs	0.38545(8)		0.49985(8)	8.2	[a]
10	NiGe	$Pnma$	MnP	0.5389	0.3438	0.5820		[9–12,23,24]
	NiGe	$Pnma$	MnP	0.53976(19)	0.34279(9)	0.58250(16)	8.9	[a]
11	Ho_5Ge_3	$P6_3/mcm$	Mn_5Si_3	0.8400		0.6300		[9–12,23,25]
	Ho_5Ge_3	$P6_3/mcm$	Mn_5Si_3	0.83813(9)		0.62638(7)	1.3	[a]
12	Ho_5Ge_4	$Pnma$	Sm_5Ge_4	0.7540	1.4510	0.7630		[9–12,23,25]
	Ho_5Ge_4	$Pnma$	Sm_5Ge_4	0.7585(2)	1.4560(3)	0.7656(2)	7.8	[a]
13	$Ho_{11}Ge_{10}$	$I4/mmm$	$Ho_{11}Ge_{10}$	1.0790		1.6230		[9–12,23,25]
14	HoGe	$Cmcm$	CrB	0.4250	1.0620	0.3910		[9–12,23,25]
	HoGe	$Cmcm$	CrB	0.42338(4)	1.06198(13)	0.39197(4)	7.1	[a]
15	Ho_3Ge_4	$Cmcm$	Gd_3Ge_4	0.4036	1.0597	1.4163		[9–12,23,25]
16	Ho_2Ge_3 [b]	$P6/mmm$	AlB_2	0.3900		0.4110		[9–12,23,25]
17	Ho_3Ge_5	$Fdd2$	Y_3Ge_5	0.57158	1.71475	1.36332		[9–12,23,25]
	$HoGe_{1.7}$	$I4_1/amd$	$ThSi_2$	0.4051		1.3651		[9–12,23,25]
18	$HoGe_{1.85}$	$Cmcm$	$YGe_{1.82}$	0.40809	2.965	0.39093		[9–12,23,25]
19	$HoGe_{2.7}$	$Cmcm$	$DyGe_3$	0.3995	2.0736	0.3877		[9–12,23,25]
20	Ho_2Ni_{17}	$P6_3/mmc$	Th_2Ni_{17}	0.8290		0.8020		[9–12,23,26]
	$Ho_{11}Ni_{78}Ge_{11}$	$P6_3/mmc$	Th_2Ni_{17}	0.83321(7)		0.81224(7)	7.7	[a]
	$Ho_{11}Ni_{74}Ge_{15}$	$P6_3/mmc$	Th_2Ni_{17}	0.83594(7)		0.81349(7)	5.4	[a]
	$Ho_{12}Ni_{70}Ge_{17}$	$P6_3/mmc$	Th_2Ni_{17}	0.84018(8)		0.81171(8)	3.6	[a]
21	$HoNi_5$	$P6/mmm$	$CaCu_5$	0.4872		0.3966		[9–12,23,26]
	$Ho_{17}Ni_{69}Ge_{14}$	$P6/mmm$	$CaCu_5$	0.48960(2)		0.40109(2)	5.3	[a]
	$Ho_{17}Ni_{67}Ge_{16}$	$P6/mmm$	$CaCu_5$	0.49056(4)		0.40081(3)	5.3	[a]
22	Ho_2Ni_7	$R\bar{3}m$	Er_2Co_7	0.49210		3.6090		[9–12,23,26]
	$Ho_{23}Ni_{71}Ge_6$	$R\bar{3}m$	Er_2Co_7	0.4922(4)		3.6334(20)	5.8	[a]
23	$HoNi_3$	$R\bar{3}m$	$PuNi_3$	0.4957		2.4190		[9–12,23,26]
	$Ho_{25}Ni_{70}Ge_5$	$R\bar{3}m$	$PuNi_3$	0.49691(8)		2.43691(38)	4.6	[a]
24	$HoNi_2$	$Fd\bar{3}m$	$MgCu_2$	0.7136				[9–12,23,26]
	$Ho_{33}Ni_{65}Ge_2$	$Fd\bar{3}m$	$MgCu_2$	0.71564(9)			3.8	[a]
25	HoNi	$Pnma$	FeB	0.7022	0.4140	0.5435		[9–12,23,26]
	$Ho_{50}Ni_{47}Ge_2$	$Pnma$	FeB	0.70328(11)	0.41481(7)	0.54424(9)	6.3	[a]
26	$Ho_3Ni_{2\ LT}$	$C2/m$	Dy_3Ni_2	1.3300	0.3650 $\beta = 105.6°$	0.9510		[9–12,23,26]
	$Ho_3Ni_{2\ HT}$	$R\bar{3}$	Er_3Ni_2	0.8520		1.5750		[9–12,23,26]
27	Ho_3Ni	$Pnma$	Fe_3C	0.6830	0.9540	0.6250		[9–12,23,26]
	Ho_3Ni	$Pnma$	Fe_3C	0.6866(2)	0.9440(3)	0.6239(2)	7.9	[a]

[a] This work (the phase is detected in the ternary sample).
[b] Quasi-binary solid solution data for Ho_2Ge_3 are given in Table 2.

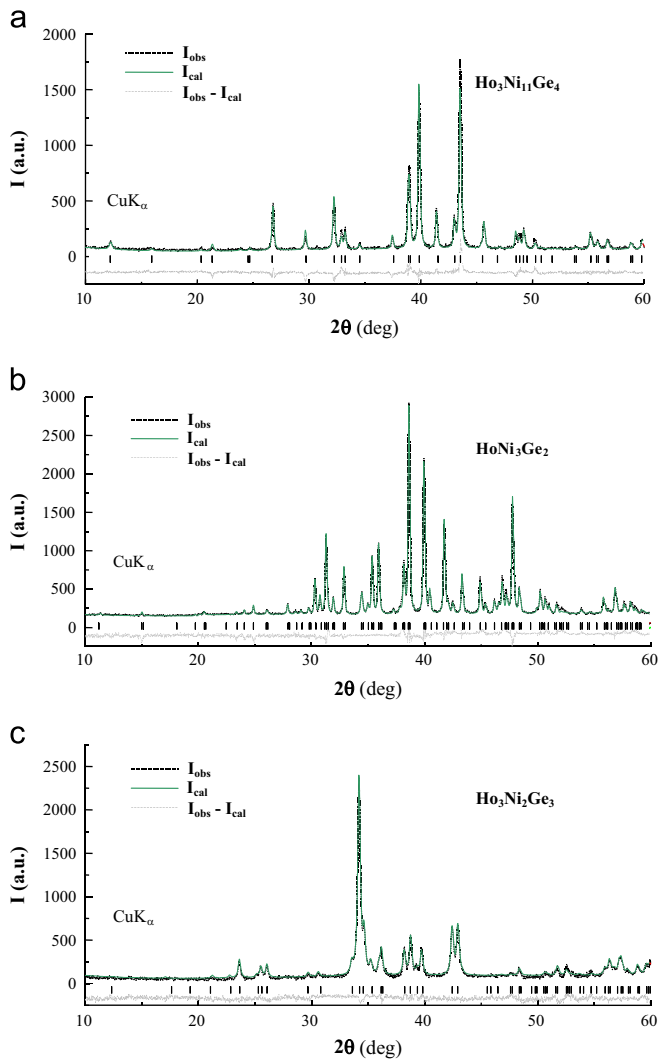

Fig. 3. Rietveld refinement plots of the (a) $Sc_3Ni_{11}Ge_4$-type $Ho_3Ni_{11}Ge_4$, (b) $ErNi_3Ge_2$-type $HoNi_3Ge_2$ and (c) $Hf_3Ni_2Si_3$-type $Ho_3Ni_2Ge_3$ compounds.

were detected, as well as an extended solid solution for the $HoNi_{0.2-0.65}Ge_2$ compound (see Fig. 1). The homogeneity range for $HoNi_{0.2-0.65}Ge_2$ was established from the microprobe and powder diffraction results. The successful Rietveld refinement indicated the $Sc_3Ni_{11}Ge_4$ ($EuMg_5$)-, $ErNi_3Ge_2$- and $Hf_3Ni_2Si_3$-type structures for the $Ho_3Ni_{11}Ge_4$, $HoNi_3Ge_2$ and $Ho_3Ni_2Ge_3$ compounds, respectively (Fig. 3). The crystal structure of the ~$Ho_5Ni_2Ge_3$ compound remains uncertain; further experimental investigations on the formation of this phase are ongoing. The crystallographic data and refined lattice parameters of these compounds are summarized in Table 2.

3.2. Crystal structure of the new compounds in the rare earth–Ni–Ge systems

3.2.1. {Ho, Er}$_3$Ni$_{11}$Ge$_4$ compounds

Rietveld analysis of the {Ho, Er}$_3$Ni$_{11}$Ge$_4$ phases showed that they crystallize with the $Sc_3Ni_{11}Ge_4$-type structure and, thus, are isomorphic with the other known compounds belonging to the 3:11:4 family, formed by Sc, Y, Tb, Dy, Tm–Lu [4–8,12]. The lattice parameters, obtained from the X-ray powder diffraction, are given in Table 3a; as it can be seen, they show a regular trend along the series in agreement with the lanthanide contraction [35]. The interatomic distances calculated for the $Ho_3Ni_{11}Ge_4$ compound are reported in Table 3b. The small deviation with respect to the sum of metallic radii of Ho, Ni and Ge [27,36] suggests a metallic bonding in this compound; the same assumption can be made for the other isotypic compounds. The phase '$Gd_3Ni_{11}Ge_4$' could not be obtained under the present synthetic conditions; the '$Gd_3Ni_{11}Ge_4$' alloy was a mixture of three phases, which were identified as $GdNi_2Ge_2$ ($CeAl_2Ga_2$-type), $GdNi_5Ge_3$ (YNi_5Si_3-type) and $GdNi_{5-x}Ge_x$ ($CaCu_5$-type) [9–14].

3.2.2. {Y, Yb, Ho}Ni$_3$Ge$_2$ compound

Rietveld analysis of the new {Y, Ho, Yb}Ni_3Ge_2 phases indicated that they adopt the $ErNi_3Ge_2$ structure, which can be considered as an ordered superstructure derived from the $CaCu_5$ structure type. The atomic positions of the prototype $ErNi_3Ge_2$ [21] were used as a model for the powder data refinement of the Y, Ho and Yb analogs (see for example Fig. 3b). The corresponding lattice parameters, together with those of the already known compounds (R=Er, Tm) [5,12,21] are listed in Table 4. The formation of the $DyNi_3Ge_2$ phase has not been observed; instead, the '$DyNi_3Ge_2$' alloy was a mixture of the known $CeAl_2Ga_2$-type $DyNi_2Ge_2$, YNi_5Si_3-type $DyNi_5Ge_3$ and $EuMg_5$-type $Dy_3Ni_{11}Ge_4$ phases [4,9–14].

3.2.3. R$_3$Ni$_2$Ge$_3$ compounds (R=Y, Tb–Tm)

The {Y, Tb–Tm}$_3$Ni$_2$Ge$_3$ compounds ($Hf_3Ni_2Si_3$-type) are isostructural with $Lu_3Ni_2Ge_3$ [12,22]. The lattice parameters of the $R_3Ni_2Ge_3$ phases obey the lanthanide contraction rule [35] (Table 5a). Interatomic distances in $R_3Ni_2Ge_3$ suggest a metallic bonding as shown for $Tb_3Ni_2Ge_3$ in Table 5b. A sample with a nominal composition '$Gd_3Ni_2Ge_3$' was prepared to check the formation of the same structure for the lighter rare earths, however we could not obtain this compound; the corresponding '$Gd_3Ni_2Ge_3$' alloy contained three phases, CrB-type GdGe, TiNiSi-type GdNiGe and AlB_2-type $GdNi_{0.6}Ge_{1.4}$ [9–12].

3.3. Magnetic properties of HoNi$_5$Ge$_3$, Ho$_3$Ni$_2$Ge$_3$ and Ho$_3$Ni$_{11}$Ge$_4$ (with isostructural {Tb, Dy}$_3$Ni$_{11}$Ge$_4$)

According to the temperature dependence of the DC magnetization, the YNi_5Si_3-type $HoNi_5Ge_3$ and $ErNi_3Ge_2$-type $HoNi_3Ge_2$ phases show no magnetic ordering down to 5 K (Fig. 4a and b). However, a slight upturn of the data below 20 K for $HoNi_5Ge_3$ and below 40 K for $HoNi_3Ge_2$ suggests a likely magnetic transition below 5 K. The inverse susceptibility, $1/\chi$, of $HoNi_5Ge_3$ and $HoNi_3Ge_2$ follows the Curie–Weiss law from 20 K and from 40 K to 300 K, respectively (inset of Fig. 4a and b). From the Curie–Weiss fits, an effective paramagnetic moment M_{eff}=10.76 μ_B/Ho with a paramagnetic temperature θ_P=−2.1 K and M_{eff}=10.86 μ_B/Ho with θ_P=−3.1 K were obtained for $HoNi_5Ge_3$ and $HoNi_3Ge_2$, respectively. The experimental magnetic moments are only slightly higher than the theoretical value of 10.61 μ_B [37] for the free Ho^{3+} ions, and such enhancement may come from the polarization of the conduction Ho d electrons by the localized 4f-electron magnetic moments. Ni is unlikely to carry magnetic moments as its 3d states will be filled. The negative paramagnetic temperatures suggest possible antiferromagnetic transitions of $HoNi_5Ge_3$ and $HoNi_3Ge_2$ below 5 K.

The DC magnetization for $Ho_3Ni_2Ge_3$, measured between 5 and 300 K, is shown in Fig. 4c. The inverse magnetic susceptibility follows the Curie–Weiss law in the temperature range from 50 to 300 K (inset of Fig. 4c); the fit yields an effective magnetic moment M_{eff}=10.76 μ_B/Ho, which is again close to the theoretical value for the free Ho^{3+} ion [37]. Similarly to both $HoNi_5Ge_3$ and $Ho_3Ni_2Ge_3$, there can be some contribution from the polarized Ho d electrons in $Ho_3Ni_2Ge_3$. Even though the nature of the magnetic transition in $Ho_3Ni_2Ge_3$ cannot be established with certainty (there are not

Table 2
Crystal data of the ternary compounds in the Ho–Ni–Ge system.

N [a-]	Compound	Space group	Type structure	*a* (nm)	*b* (nm)	*c* (nm)	R_F (%)	Refs.
1	$HoNi_5Ge_3$	*Pnma*	YNi_5Si_3	1.9067	0.38583	0.6790		[9–13]
				1.90658(8)	0.38562(1)	0.67931(3)	3.1	[b-]
2	$Ho_3Ni_{11}Ge_4$	$P6_3/mmc$	$Sc_3Ni_{11}Ge_4$	0.82768(7)		0.86770(5)	6.0	[b-]
3	$HoNi_3Ge_2$	$P\bar{6}$	$ErNi_3Ge_2$	1.79988(6)		0.38020(1)	2.6	[b-]
4	$HoNi_2Ge_2$	*I4/mmm*	$CeAl_2Ga_2$	0.4021		0.9757		[9–12,14]
				0.40291(2)		0.97703(7)	6.8	[b-]
5	$HoNiGe_3$	*Cmmm*	$SmNiGe_3$	0.40061	2.13830	0.40305		[9–12,15]
				0.40334(6)	2.14535(22)	0.40406(6)	5.4	[b-]
6	$HoNi_{0.6}Ge_2$	*Cmcm*	$CeNiSi_2$	0.3993(3)	1.5989(16)	0.4031(2)		[9–12,16]
	$HoNi_{0.66}Ge_2$	*Cmcm*	$CeNiSi_2$	0.40843(4)	1.63069(13)	0.40207(4)	3.1	[b-]
	$HoNi_{0.53}Ge_2$	*Cmcm*	$CeNiSi_2$	0.40842(2)	1.61262(9)	0.39986(2)	6.7	[b-]
	$HoNi_{0.49}Ge_2$	*Cmcm*	$CeNiSi_2$	0.40858(3)	1.61205(11)	0.39995(3)	6.2	[b-]
	$HoNi_{0.41}Ge_2$	*Cmcm*	$CeNiSi_2$	0.40761(2)	1.60128(9)	0.39767(3)	5.8	[b-]
	$HoNi_{0.19}Ge_2$	*Cmcm*	$CeNiSi_2$	0.40583(3)	1.58379(14)	0.39356(3)	8.5	[b-]
7	Ho_2NiGe_6	*Amm2*	Ce_2CuGe_6	0.4003	0.3947	2.1157		[9–12,17]
				0.40079(3)	0.39590(3)	2.11969(19)	9.0	[b-]
8	HoNiGe	*Pnma*	TiNiSi	0.6856	0.42040	0.7256		[9–12,18]
				0.68665(4)	0.42048(3)	0.72586(6)	3.3	[b-]
9	$HoNi_{0.5}Ge_{1.5}$ [c-]	*P6/mmm*	AlB_2	0.4060		0.3970		[9,12,19]
	$Ho_{37}Ni_6Ge_{57}$ [c-]	*P6/mmm*	AlB_2	0.39827(4)		0.40482(3)	4.7	[b-]
	$Ho_{38}Ni_{12}Ge_{50}$ [c-]	*P6/mmm*	AlB_2	0.40265(2)		0.40130(2)	4.1	[b-]
	$Ho_{35}Ni_{17}Ge_{48}$ [c-]	*P6/mmm*	AlB_2	0.40656(2)		0.39786(1)	5.2	[b-]
	$Ho_{34}Ni_{20}Ge_{46}$ [c-]	*P6/mmm*	AlB_2	0.40796(3)		0.39488(3)	2.3	[b-]
	$Ho_{34}Ni_{24}Ge_{42}$ [c-]	*P6/mmm*	AlB_2	0.41517(29)		0.39304(30)	4.7	[b-]
10	$Ho_3Ni_2Ge_3$	*Cmcm*	$Hf_3Ni_2Si_3$	0.41693(4)	1.02484(8)	1.39966(13)	4.5	[b-]
11	Ho_3NiGe_2	*Pnma*	La_3NiGe_2	1.1195	0.4197	1.1192		[9–12,20]
				1.12835(4)	0.41471(1)	1.11307(4)	4.0	[b-]
12	$Ho_5Ni_2Ge_3$	...	*unknown*					[b-]

[a-] Numbers match the ternary phases in Fig. 1.
[b-] This work.
[c-] Compositions belonging to the extended quasi-binary solid solution of Ho_2Ge_3.

Table 3a
Lattice and Rietveld refinement parameters for $Sc_3Ni_{11}Ge_4$-type $R_3Ni_{11}Ge_4$ (R=Sc, Y, Tb–Lu, space group $P6_3/mmc$, N 194, $hP36$).

Compound	*a* (nm)	*c* (nm)	*c*/*a*	*V* (nm^3)	R_F (%)	Refs.
$Sc_3Ni_{11}Ge_4$	0.8130	0.8505	1.04613	0.48684		[8,12]
$Y_3Ni_{11}Ge_4$	0.8319	0.8821	1.06034	0.52868		[4,12]
$Y_3Ni_{11}Ge_4$	0.83039(5)	0.87018(5)	1.04792	0.51964	2.9	[b-]
$Tb_3Ni_{11}Ge_4$ [-]	0.8321	0.8832	1.06141	0.52959		[4,12]
$Tb_3Ni_{11}Ge_4$	0.83101(6)	0.87154(4)	1.04877	0.52123	3.8	[b-]
$Dy_3Ni_{11}Ge_4$	0.8317	0.8807	1.05892	0.52758		[4,12]
$Dy_3Ni_{11}Ge_4$	0.82963(6)	0.86940(5)	1.04794	0.51823	3.5	[b-]
$Ho_3Ni_{11}Ge_4$ [a-]	0.82768(7)	0.86770(5)	1.04835	0.51478	4.0	[b-]
$Er_3Ni_{11}Ge_4$	0.82735(5)	0.86612(4)	1.04686	0.51344	3.6	[b-]
$Tm_3Ni_{11}Ge_4$	0.8279	0.8690	1.04964	0.51583		[5,12]
$Tm_3Ni_{11}Ge_4$	0.82634(6)	0.86467(4)	1.04639	0.51133	5.3	[b-]
$Yb_3Ni_{11}Ge_4$	0.8259	0.8648	1.04710	0.51086		[6,12]
$Lu_3Ni_{11}Ge_4$	0.8249	0.8641	1.04752	0.50921		[7,12]

[a-] Atomic parameters for $Ho_3Ni_{11}Ge_4$: Ho1 6*h* [0.1887(2), 2*x*, 1/4], Ni1 12*k* [0.1636(3), 2*x*, 0.5857(3)], Ni2 6*h* [0.5674(4), 2*x*, 1/4], Ni3 4*f* [1/3, 2/3, 0], Ge1 6*g* [1/2, 0, 0], Ge2 2*a* [0, 0, 0], $\beta_{11}=\beta_{22}=0.004866$, $\beta_{12}=0.002433$, $\beta_{33}=0.003320$, $\beta_{11}=\beta_{22}=B_{11}/(3a^2)$, $\beta_{12}=B_{11}/(6a^2)$, $\beta_{33}=B_{33}/(2c^2)$.
[b-] This work.

Table 3b
Interatomic distances in the $Sc_3Ni_{11}Ge_4$-type $Ho_3Ni_{11}Ge_4$ phases (ESD ± 0.0004 nm). Their ratio to the sum of the atomic radii of the corresponding elements is given as $\Delta=D/(r_{atom1}+r_{atom2})$; $r_{Ho}=0.17658$ nm, $r_{Ni}=0.12459$ nm, $r_{Ge}=0.1225$ nm [27,36]; **CN** is the coordination number.

Atom-	Atom	*D* (nm)	*Δ*	Atom-	Atom	*D* (nm)	*Δ*	Atom-	Atom	*D* (nm)	*Δ*
Ho -	4Ni1	0.29166	0.97	Ni1 -	1Ge2	0.24604	1.00	Ni2 -	2Ge1	0.23747	0.96
Ho -	2Ni2	0.29328	0.97	Ni1 -	2Ge1	0.25236	1.02	Ni2 -	2Ni2	0.24648	0.99
Ho -	2Ni1	0.29350	0.97	Ni1 -	2Ni2	0.25526	1.02	Ni2 -	4Ni1	0.25526	1.02
Ho -	2Ni3	0.30008	1.00	Ni1 -	1Ni3	0.25444	1.02	Ni2 -	2Ni3	0.25944	1.04
Ho -	4Ge1	0.31240	1.04	Ni1 -	2Ni1	0.27771	1.11	Ni2 -	2Ho	0.29328	0.97
Ho -	2Ge2	0.34675	1.16	Ni1 -	1Ni1	0.28513	1.14			**CN=12**	
Ho -	2Ho	0.35913	1.02	Ni1 -	2Ho	0.29166	0.97				
		CN=18		Ni1 -	1Ho	0.29350	0.97	Ge2 -	6Ni1	0.24604	1.00
						CN=12		Ge2 -	3Ho	0.34675	1.16
Ni3 -	3Ge1	0.23893	0.97	Ge1 -	2Ni2	0.23747	0.96			**CN=9**	
Ni3 -	3Ni1	0.25444	1.02	Ge1 -	2Ni3	0.23893	0.97				
Ni3 -	3Ni2	0.25944	1.04	Ge1 -	4Ni1	0.25236	1.02				
Ni3 -	3Ho	0.30008	1.00	Ge1 -	4Ho	0.31240	1.04				
		CN=12				**CN=12**					

Table 4
Lattice parameters and refinement agreement factors for RNi_3Ge_2 ($ErNi_3Ge_2$-type structure, $P\bar{6}$, *N* 174, *hP*72).

Compound	*a* (nm)	*c* (nm)	*c*/*a*	*V* (nm^3)	R_F (%)	Refs.
YNi_3Ge_2 [a-]	1.80371(16)	0.38073(2)	0.21108	1.07271	3.0	[b-]
$HoNi_3Ge_2$ [a-]	1.79988(6)	0.38020(1)	0.21124	1.06667	2.6	[b-]
$ErNi_3Ge_2$	1.79662	0.379410	0.21118	1.06060		[12,21]
$TmNi_3Ge_2$	1.78950	0.37890	0.21174	1.05080		[5,12]
$YbNi_3Ge_2$ [a-]	1.79116(8)	0.37918(1)	0.21169	1.05353	2.6	[b-]

[a-]Atomic positions of isostructural $ErNi_3Ge_2$ [21] were used for RNi_3Ge_2, *R*={Y, Ho, Yb}: *R*1 3*k* [0.0088, 0.5756, 1/2], *R*2 3*k* [0.0969, 0.3366, 1/2], *R*3 3*k* [0.3345, 0.1678, 1/2], *R*4 1*e* [2/3, 1/3, 0], *R*5 1*d* [1/3, 2/3, 1/2], *R*6 1*a* [0, 0, 0], Ni1 3*k* [0.0906, 0.1590, 1/2], Ni2 3*k* [0.2404, 0.2725, 1/2], Ni3 3*k* [0.4229, 0.0487, 1/2], Ni4 3*k* [0.5817, 0.1831, 1/2], Ni5 3*j* [0.0571, 0.4501, 0], Ni6 3*j* [0.1759, 0.6205, 0], Ni7 3*j* [0.1918, 0.0037, 0], Ni8 3*j* [0.1962, 0.1541, 0], Ni9 3*j* [0.2168, 0.4970, 0], Ni10 3*j* [0.2602, 0.3850, 0], Ni11 3*j* [0.4650, 0.1803, 0], Ni12 3*j* [0.4747, 0.3216, 0], Ge1 3*k* [0.1405, 0.5176, 1/2], Ge2 3*k* [0.1480, 0.0690, 1/2], Ge3 3*k* [0.2827, 0.4804, 1/2], Ge4 3*k* [0.5217, 0.2698, 1/2], Ge5 3*j* [0.1457, 0.2482, 0], Ge6 3*j* [0.3272, 0.2933, 0], Ge7 3*j* [0.3363, 0.0410, 0], Ge8 3*j* [0.5241, 0.0853, 0].
[b-] This work.

Table 5a
Unit cell data of $Hf_3Ni_2Si_3$-type $R_3Ni_2Ge_3$ (*R*=Y, Tb–Tm, Lu, space group *Cmcm*, *N* 63, *oC*32).

Compound	*a* (nm)	*b* (nm)	*c* (nm)	*V* (nm^3)	R_F (%)	Refs.
$Y_3Ni_2Ge_3$	0.41888(1)	1.03078(5)	1.40633(5)	0.607216	3.1	[b-]
$Tb_3Ni_2Ge_3$ [a-]	0.42002(3)	1.03333(8)	1.41055(11)	0.612206	4.1	[b-]
$Dy_3Ni_2Ge_3$	0.41903(6)	1.02846(19)	1.40460(21)	0.605320	4.4	[b-]
$Ho_3Ni_2Ge_3$	0.41694(4)	1.02487(9)	1.39977(10)	0.598135	4.5	[b-]
$Er_3Ni_2Ge_3$	0.41613(2)	1.01978(5)	1.39298(7)	0.591126	4.3	[b-]
$Tm_3Ni_2Ge_3$	0.41498(3)	1.01573(7)	1.38657(9)	0.584450	6.4	[b-]
$Lu_3Ni_2Ge_3$	0.4140	1.0103	1.3789	0.576745		[7, 22]

[a-] Atomic positions of $Tb_3Ni_2Ge_3$: Tb1 8*f* [0, 0.4117(3), 0.1099(2)], Tb2 4*c* [0, 0.1286(4), 1/4], Ni 8*f* [0, 0.7057(8), 0.0999(6)], Ge1 4*c* [0, 0.8315(9), 1/4], Ge2 8*f* [0, 0.1248(5), 0.0416(4)], $\beta_{11}=0.014171$, $\beta_{22}=0.002341$, $\beta_{33}=0.001257$ ($\beta_{11}=B_{11}/(2a^2)$, $\beta_{22}=B_{22}/(2b^2)$, $\beta_{33}=B_{33}/(2c^2)$).
[b-] This work.

Table 5b
Interatomic distances in the $Tb_3Ni_2Ge_3$ compound, $Hf_3Ni_2Si_3$-type (ESD ± 0.0005 nm). Their ratio to the sum of the atomic radii of the corresponding elements is given as $\Delta=D/(r_{atom1}+r_{atom2})$; $r_{Tb}=0.17788$ nm, $r_{Ni}=0.12459$ nm, $r_{Ge}=0.1250$ nm [27,36]; **CN** is the coordination number.

Atom	- Atom	*D* (nm)	*Δ*	Atom	- Atom	*D* (nm)	*Δ*	Atom	- Atom	*D* (nm)	*Δ*
Tb1 -	2Ge1	0.30004	1.00	Tb2 -	2Ge2	0.29398	0.98	Ni -	2Ge2	0.24053	0.97
Tb1 -	2Ge2	0.30198	1.01	Tb2 -	2Ge1	0.29675	0.99	Ni -	1Ge1	0.24845	1.01
Tb1 -	2Ni	0.29936	0.99	Tb2 -	1Ge1	0.30700	1.02	Ni -	1Ge2	0.26555	1.07
Tb1 -	1Ni	0.30413	1.01	Tb2 -	4Ni	0.30867	1.02	Ni -	2Tb1	0.29936	0.99
Tb1 -	1Ge2	0.31172	1.04	Tb2 -	2Tb1	0.35303	0.99	Ni -	1Tb1	0.30413	1.01
Tb1 -	2Ge2	0.31918	1.06	Tb2 -	4Tb1	0.36523	1.03	Ni -	2Tb2	0.30867	1.02
Tb1 -	1Ni	0.31983	1.06			**CN=15**		Ni -	1Tb1	0.31983	1.06
Tb1 -	1Tb2	0.35303	0.99							**CN=10**	
Tb1 -	1Tb1	0.35976	1.01	Ge1 -	2Ni	0.24845	1.01				
Tb1 -	2Tb2	0.36523	1.03	Ge1 -	2Tb2	0.29675	0.99	Ge2 -	2Ni	0.24053	0.97
Tb1 -	1Tb1	0.39524	1.11	Ge1 -	4Tb1	0.30004	1.00	Ge2 -	1Ni	0.26555	1.07
		CN=16		Ge1 -	1Tb2	0.30700	1.02	Ge2 -	1Ge2	0.28336	1.16
						CN=9		Ge2 -	1Tb2	0.29398	0.98
								Ge2 -	2Tb1	0.30198	1.01
								Ge2 -	1Tb1	0.31172	1.04
								Ge2 -	2Tb1	0.31918	1.06
										CN=10	

enough data points at lower temperatures), both the shape of the magnetization curve and a negative paramagnetic temperature $\theta_P=-2.9$ K indicate that $Ho_3Ni_2Ge_3$ may order antiferromagnetically with $T_N\sim7$ K.

The DC magnetization of $Sc_3Ni_{11}Ge_4$-type $Tb_3Ni_{11}Ge_4$, $Dy_3Ni_{11}Ge_4$ and $Ho_3Ni_{11}Ge_4$ does not show magnetic ordering down to 5 K (Fig. 5). However, the upturn of the data below ~30 K for $Tb_3Ni_{11}Ge_4$, $Dy_3Ni_{11}Ge_4$ and $Ho_3Ni_{11}Ge_4$ suggests a likely magnetic transition below 5 K and the inverse susceptibility, $1/\chi$, of these compounds follows the Curie–Weiss law from from ~30 K to 300 K (inset of Fig. 5a–c). From the linear fit of the data, effective paramagnetic moments for $Tb_3Ni_{11}Ge_4$, $Dy_3Ni_{11}Ge_4$ and $Ho_3Ni_{11}Ge_4$ are M_{eff}/fu=17.07 μ_B (M_{eff}/Tb=9.85 μ_B), M_{eff}/fu=18.88 μ_B (M_{eff}/Dy=10.90 μ_B) and M_{eff}/fu=18.91 μ_B (M_{eff}/Ho=10.91 μ_B), respectively. The experimental magnetic moments slightly higher than the theoretical value of terbium (9.72 μ_B), dysprosium (10.65 μ_B) and holmium (10.61 μ_B) [37] for free R^{3+} ions, which may come from the polarization of the conduction rare-earth *d* electrons by localized 4*f*-electron magnetic moments. Again Ni should not give any contribution to the magnetic moments due to its fully occupied *d* states.

The positive paramagnetic temperatures of 3.7 K, 3.1 K and 1.5 K for $Tb_3Ni_{11}Ge_4$, $Dy_3Ni_{11}Ge_4$ and $Ho_3Ni_{11}Ge_4$, respectively, suggest possible ferromagnetic transitions in these compounds below 5 K.

The magnetic data for the ternary compounds in the Ho–Ni–Ge system and {Tb, Dy}$_3Ni_{11}Ge_4$ compounds (paramagnetic temperatures,

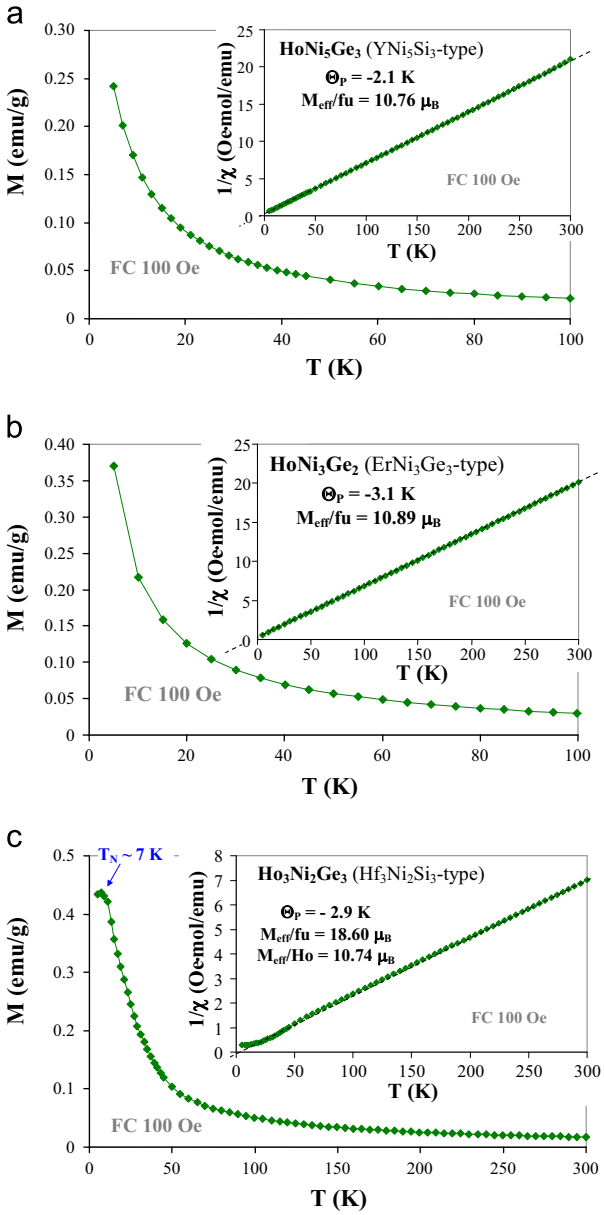

Fig. 4. Magnetization as a function of temperature measured on field cooling at 100 Oe of (a) $HoNi_5Ge_3$ (b) $HoNi_3Ge_2$ and (c) $Ho_3Ni_2Ge_3$ compounds; the inset shows the inverse magnetic susceptibility.

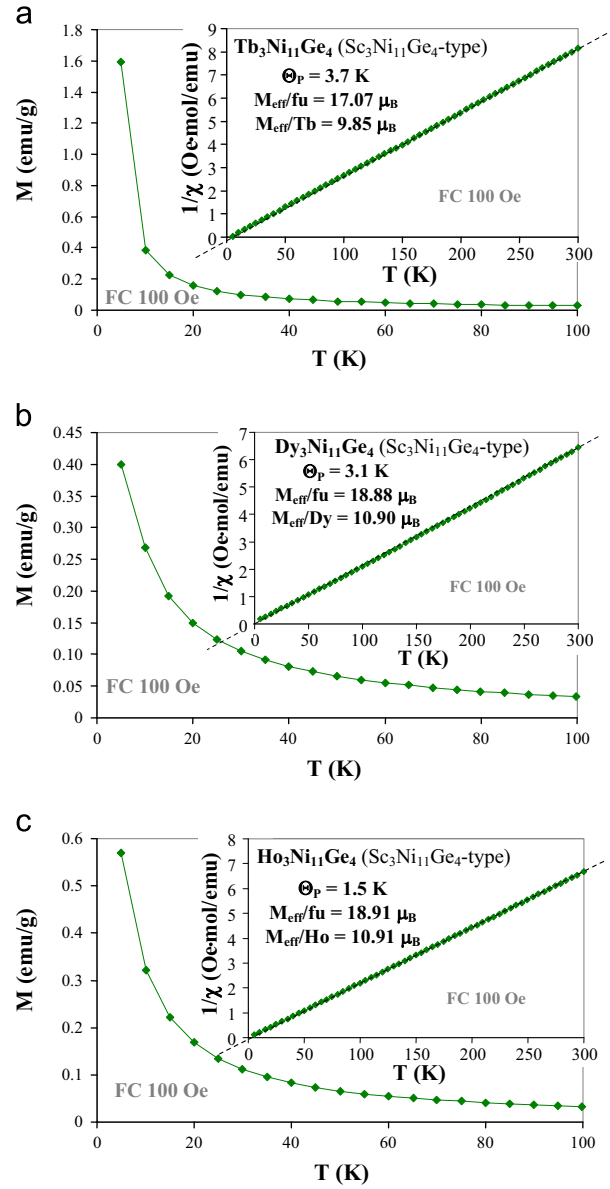

Fig. 5. Magnetization as a function of temperature measured on field cooling at 100 Oe of (a) $Tb_3Ni_{11}Ge_4$, (b) $Dy_3Ni_{11}Ge_4$ and (c) $Ho_3Ni_{11}Ge_4$ compounds; the inset shows the inverse magnetic susceptibility.

effective magnetic moments and magnetic ordering temperatures) are summarized in Table 6.

4. Discussion and conclusions

The current investigation of the Ho–Ni–Ge system expands the series of the *R*–Ni–Ge systems, for which the isothermal sections have been previously constructed. The novel ternary phases discovered in the system also expand the family of the isostructural rare-earth–nickel germanides. A distribution map of the crystal structures along the entire lanthanide series, including La, Y and Sc, is summarized in Table 7. The rare-earth sequence in this table (Eu–La–Ce–Pr–Nd–Sm–Gd–Tb–Dy–Y–Ho–Er–Tm–Yb–Lu–Sc) has been intentionally chosen as it represents a systematic decrease in the unit cell parameters of the isostructural compounds (including Yb when in the trivalent state). This sequence mirrors the W→α-La→Sm→Mg structural sequence observed for pure rare-earth metals and one could argue that this sequence influences the structure of the binary and ternary compounds as well. Knowledge on the known ternary rare-earth compounds (Table 7) can be used to predict the formation of isostoichiometric and isostructural compounds in other systems; in fact, in the new compounds identified in this study were anticipated based on the similar crystallographic and physicochemical behavior of neighboring rare earths. Following this argument about the similarity across the lanthanide series, we can predict the existence of the $LuNi_3Ge_2$ and $Yb_3Ni_2Ge_3$ compounds ($ErNi_3Ge_2$-type and $Hf_3Ni_2Si_3$-type, respectively), and of the ~{Dy, Er}$_5Ni_2Ge_3$ phases (yet with unknown crystal structure).

The magnetic measurements on $HoNi_5Ge_3$, $HoNi_3Ge_2$, $Ho_3Ni_{11}Ge_4$ and $Ho_3Ni_2Ge_3$ supplement our knowledge on the magnetic behavior of the ternary compounds in the Ho–Ni–Ge system. In general, Ho-rich and Ni-rich phases in the Ho–Ni–Ge system have dominant ferromagnetic ground state interactions, while the

Table 6
Weiss temperatures Θ_P, effective magnetic moments per rare-earth atom M_{eff}/R, and ordering temperatures (antiferro T_N, mixed ferro-antiferro T_{CN}) of holmium nickel germanides.

Compound	Type structure	Θ_P (K)	M_{eff}/R (μ_B)	Ordering temperature	Refs.
$Tb_3Ni_{11}Ge_4$	$Sc_3Ni_{11}Ge_4$	3.7	9.85	–	[a]
$Dy_3Ni_{11}Ge_4$	$Sc_3Ni_{11}Ge_4$	3.1	10.90	–	[a]
$Ho_3Ni_{11}Ge_4$	$Sc_3Ni_{11}Ge_4$	1.5	10.91	–	[a]
$HoNi_5Ge_3$	YNi_5Ge_3	−2.1	10.76	–	[a]
$HoNi_3Ge_2$	$ErNi_3Ge_2$	−3.1	10.89	–	[a]
$HoNi_2Ge_2$	$CeAl_2Ga_2$	1.0	10.27	T_N=4.8 K	[12,28]
$HoNiGe_3$	$SmNiGe_3$	−3.9	10.69	T_N=10 K	[38]
$HoNi_{0.6}Ge_2$	$CeNiSi_2$			T_N=11 K	[39]
Ho_2NiGe_6	Ce_2CuGe_6	−11	10.58	T_N=14 K	[12,29]
HoNiGe	TiNiSi	−3.7	10.43		[12,30]
Ho_2NiGe_3	AlB_2	…	…	…	[19]
$Ho_3Ni_2Ge_3$	$Hf_3Ni_2Si_3$	−2.9	10.74	T_N=7 K	[a]
Ho_3NiGe_2	La_3NiGe_2	30.2	10.61	T_{CN}=43 K	[31]

[a] This work.

Table 7
Ternary compounds and their type structure in the *R*–Ni–Ge systems.

				→ Decreasing of unit cell parameters of the compound →															
RT Type structure of Rare Earth →				*W*	*α*-La				Sm	Mg									
R **(at%)**	**Compound**	**Structure**	**Space group**	**Eu**	**La**	**Ce**	**Pr**	**Nd**	**Sm**	**Gd**	**Tb**	**Dy**	**Y**	**Ho**	**Er**	**Tm**	**Yb**	**Lu**	**Sc**
7.14	$RNi_{8.5}Ge_{4.5}$	$LaCo_9Si_4$	*I*4/*mcm*	+	+	+	+	+	+										
7.69	RNi_6Ge_6	$ScNi_6Ge_6$	*P*6/*mmm*																+
11.11	RNi_5Ge_3	YNi_5Si_3	*Pnma*						+	+	+	+	+	+	+	+	+	+	
12.50	$R_2Ni_9Ge_5$	*Unknown*							+										
14.29	RNi_3Ge_3	$SmNi_3Ge_3$	*I*4/*mmm*						+										
16.67	RNi_3Ge_2	$ErNi_3Ge_2$	$P\bar{6}$									−	⊕	⊕	+	+	⊕	→	
	$R_3Ni_{11}Ge_4$	$EuMg_5$	$P6_3/mmc$							−	+	+	+	⊕	⊕	+	+	+	+
20.00	RNi_2Ge_2	$CeAl_2Ga_2$	*I*4/*mmm*	+	+	+	+	+	+	+	+	+	+	+	+	+	+	+	
	$R_2Ni_3Ge_5$	$U_2Co_3Si_5$	*Ibam*			+	+												
		Unknown					+	+											
	$RNiGe_3$	$SmNiGe_3$	*Cmmm*			+	+	+	+	+	+	+	+	+	+				
		$ScNiSi_3$	*Amm*2				+				+	+	+						
		$LuNi_{1-x}Ge_3$	*C*2/*m*													+		+	
		$YbNiGe\sim_3$	$I4_1/amd$														+		
		$BaNiSn_3$	*I*4*mm*	+															
20.69	$R_6Ni_{16}Ge_7$	Th_6Mn_{23}	$Fm\bar{3}m$																+
22.22	R_2NiGe_6	Ce_2CuGe_6	*Amm*2			+	+	+	+	+	+	+	+	+	+	+	+	+	
25.00	$RNi_{1-x}Ge_2$	$CeNiSi_2$	*Cmcm*	+	+	+	+	+	+	+	+	+	+	+	+	+	+	+	
	$R_3Ni_2Ge_7$	$La_3Co_2Sn_7$	*Cmmm*			+													
27.27	$R_3Ni_4Ge_4$	$U_3Ni_4Si_4$	*Immm*		+	+	+												+
33.33	*R*NiGe	TiNiSi	*Pnma*			+	+	+	+	+	+	+	+	+	+	+	+	+	
		EuNiGe	$P2_1/b$	+															
	RNi_xGe_{2-x}	AlB_2	*P*6/*mmm*	+	+	+	+	+	+	+	+	+	+	+	+		+		
37.50	$R_3Ni_2Ge_3$	$Hf_3Ni_2Si_3$	*Cmcm*							−	⊕	⊕	⊕	⊕	⊕	⊕	→	+	
50.00	R_2NiGe	La_2NiGe	*I*4/*mcm*		+	+													
	$R_5Ni_2Ge_3$	*Unknown*											←	⊕	→				
	R_3NiGe_2	La_3NiGe_2	*Pnma*		+	+	+	+	+	+	+	+	+	+	+	+			
52.38	$R_{11}Ni_4Ge_6$	$Ce_{11}Ni_4Ge_6$	*C*2/*m*		+	+													
55.56	R_5NiGe_3	Hf_5CuSn_3	$P6_3/mcm$		+														
57.14	R_8NiGe_5	La_8NiGe_5	*Pmmn*		+														
62.50	R_5NiGe_2	Cr_5B_3	*I*4/*mcm*			+													

+Known compound [1-22]; ⊕new compound detected in present work; →the possible extension of compound's row; −compound was not detected in present work.

remaining phases often display antiferromagnetic orderings at low temperatures. We suggest that the magnetic behavior of the ternary compounds in the {Gd, Tb, Dy, Er, Tm}–Ni–Ge systems follows this trend as well.

Acknowledgments

This work was supported by the Russian Fund for Basic Research Grant no 12-03-00428-a.

References

[1] Y. Zhuang, Z.J. Hu, J. Liu, J. Yan Lü, J. Alloy. Compd. 387 (2005) 239–242.
[2] P.S. Salamakha, M.B. Konyk, O.L. Sologub, O.I. Bodak, J. Alloy. Compd. 236 (1996) 206–211.
[3] M.F. Fedyna, V.K. Pecharskii, O.I. Bodak, Dopov. Akad. Nauk Ukr. RSR Ser. B 2 (1987) 50–52 (In Russian).
[4] G.M. Koterlyn, P.K. Starodub, G.I. Kirchiv, O.I. Bodak, Visn. Lviv. Derzh. Univ. Ser. Khim. 29 (1988) 56–62 (In Russian).
[5] M.F. Fedyna, O.I. Bodak, I.R. Mokra, Metally 2 (2001) 118–123 (In Russian).
[6] R.B. Dzyanyi, O.I. Bodak, V.V. Pavlyuk, Russ. Metall. 4 (1995) 133–135 (In Russian).

[7] O.I. Bodak, G.M. Koterlyn, in: Proc. 6th Int. Conf. Cryst. Chem. Intermet. Compd., 1995, p. 26.
[8] B.Y. Kotur, R.I. Andrusyak, Inorg. Mater. 27 (1991) 1207–1212.
[9] Pearson's Handbook of Crystallographic Data for Intermetallic Phases, American Society for Metals, Metals Park, OH 44073, vol. 1–3, 1985.
[10] P. Villars, K. Cenzual, PCD Pearson's Crystal Data, Crystal Structure Database for Inorganic Compounds, release 2013/2014.
[11] E.I. Gladyshevskyi, O.I. Bodak, Kristallochimia intermetallicheskih soedinenii redkozemel'nyh metallov, Lviv, Vischa shkola, 1982, p. 255 (In Russian).
[12] SpringerMaterials The Landolt-Börnstein Database – Materials Science Data for 250000 Substances, ⟨http://www.springermaterials.com⟩.
[13] J.T. Zhao, B. Chabot, E. Parthé, Acta Crystallogr. C 43 (1987) 1458–1461.
[14] W. Rieger, E. Parthé, Mon. Chem. 100 (1969) 444–454.
[15] O.I. Bodak, V.K. Pecharskii, O.Y. Mrooz, V.E. Zavodnik, G.M. Vitvitskaya, P.S. Salamakha, Dopov. Akad. Nauk Ukr. RSR, Ser. B 2 (1985) 36–38 (In Russian).
[16] O.I. Bodak, E.I. Gladyshevsky, Kristallografiya 14 (1969) 990 (In Russian).
[17] E.I. Gladyshevsky, O.I. Bodak, V.K. Pecharsky, Handbook on Physics and Chemistry of Rare Earth, vol. 13, Elsevier, Amsterdam (1990) 1–190.
[18] Y.K. Gorelenko, P.K. Starodub, V.A. Bruskov, R.V. Skolozdra, V.I. Yarovets, O. I. Bodak, V.K. Pecharskii, Ukr. Fiz. Zh. Russ. Ed. 29 (1984) 867–871 (In Russian).
[19] J.W. Chen, S.Y. Guan, C.H. Wang, J. Phys. Conf. Ser. 266 (012006) (2011) 1–5.
[20] O.I. Bodak, V.A. Bruskov, V.K. Pecharskii, Sov. Phys. Crystallogr. 27 (1982) 538–540 (In Russian).
[21] O.Y. Oleksyn, O.I. Bodak, J. Alloy. Compd. 215 (1994) 45–49.
[22] G.M. Koterlyn, O.I. Bodak, V.V. Pavlyuk, J. Stepien Damm, A. Pietraszko, J. Alloy. Compd. 291 (1999) 110–116.
[23] Diagrammy sostoynia dvoinyh metallicheskih system (Diagram of binary metallic systems), Handbook, 2001, 1–3 (In Russian).
[24] A. Nash, P. Nash, Binary Alloy Phase Diagrams, II Ed., Ed. T.B. Massalski, 2 ,1990, 1974–1976.
[25] V.N. Eremenko, I.M. Obushenko, Y.I. Buyanov, Dopov. Akad. Nauk Ukr. RSR Ser. A 7 (1980) 87–91 (In Russian).
[26] H. Okamoto, J. Ph. Equilib. 13 (1992) 573–574.
[27] Emsley, The Elements, second ed., Clarendon press, Oxford, 1991.
[28] G. André, P. Bonville, F. Bourée Vigneron, A. Bombik, M. Kolenda, A. Oles, A.W. Pacyna, W. Sikora, A. Szytula, J. Alloy. Compd. 224 (1995) 253–261.
[29] M.B. Konyk, L.P. Romaka, D. Gignoux, D. Fruchart, O.I. Bodak, Y.K. Gorelenko, J. Alloy. Compd. 398 (2005) 8–11.
[30] P.A. Kotsanidis, J.K. Yakinthos, H. Gamari Seale, J. Less Common Met. 157 (1990) 295–300.
[31] A.V. Morozkin, Jinlei Yao, Fang Yuan, Y. Mozharivskyj, O. Isnard, J. Magn. Magn. Mater. 360 (2014) 200–204.
[32] F. Izumi, in: R.A. Young (Ed.), The Rietveld Method, Oxford University Press, Oxford, 1993.
[33] Bilbao Crystallographic Server [The crystallographic site at the Condensed Matter Physics Dept. of the University of the Basque Country], ⟨http://www.crys.ehu.es⟩.
[34] R.A. Levy, Principles of Solid State Physics, Academic Press, New York, 1968.
[35] J.P. Senateur, R. Fruchart, Compt. Rend. Acad. Sci. Paris 258 (1964) 1524–1525.
[36] I.S Grigor'ev, E.Z Meilohov (Eds.), Fizicheskie Velichiny (Physical Data), Energoatomizdat, Moscow, 1994 (In Russian).
[37] S. Legvold, Ferromagnetic materials, in: P. Wohlfarth (Ed.), Rare Earth Metals and Alloys, North-Holland Publ. Co., Amsterdam, 1980, pp. 183–295.
[38] E.D. Mun, S.L. Bud'ko, H. Ko, G.J. Miller, P.C. Canfield, J. Magn. Magn. Mater. 322 (2010) 3527–3543.
[39] W. Bazela, J. Leciejewicz, K. Maletka, A. Szytula, J. Magn. Magn. Mater. 109 (1992) 305–308.